

Greatly enhanced dielectric permittivity in poly(vinylidene fluoride)-based polymeric composites induced by $\text{Na}_{1/3}\text{Ca}_{1/3}\text{Bi}_{1/3}\text{Cu}_3\text{Ti}_4\text{O}_{12}$ nanoparticles

Pornsawan Kum-onsa¹ · Prasit Thongbai² · Santi Maensiri³ · Prinya Chindaprasirt⁴

Received: 15 March 2016 / Accepted: 18 May 2016 / Published online: 23 May 2016
© Springer Science+Business Media New York 2016

Abstract Greatly enhanced dielectric permittivity (ϵ') in poly(vinylidene fluoride) (PVDF) polymeric composites was induced by incorporating $\text{Na}_{1/3}\text{Ca}_{1/3}\text{Bi}_{1/3}\text{Cu}_3\text{Ti}_4\text{O}_{12}$ (NCB) nanoparticles. The NCB/PVDF composites were fabricated by conventional mixed powders and hot pressing. Nanosized (NCB-NPs) and microsized-powders (NCB-MPs) prepared, respectively, by chemical combustion and solid state reaction methods were used as fillers. The dispersion of NCB-NPs was quite **good** in the PVDF matrix. A greatly improved ϵ' of PVDF-based polymeric composites can be induced by filling with NCB-NPs compared to that of the NCB-MPs/PVDF composite. Interestingly, at 10^3 Hz, the nanocomposite with 50 vol% of NCB-NPs can exhibit good dielectric properties with high ϵ' of about 210.8 and low loss tangent ($\tan\delta \approx 0.83$). This enhanced ϵ' value is much larger than that of PVDF polymer by a factor of ≈ 20 . The increase in ϵ' in the nanocomposites is attributed to large interfacial areas and very short interparticle distance. These can cause a great increase in the interfacial polarization intensity.

1 Introduction

Polymer matrix composites with good dielectric performance have been intensively developed in recent years because of their variety potential applications, especially for microelectronics, electrical engineering, and high-energy-density storage devices [1–7]. For practical application in microelectronics, polymeric dielectric materials with high dielectric permittivity (ϵ'), low dielectric loss tangent ($\tan\delta$), mechanical flexibility, low cost, and excellent processing performance as well as compatible with polymers used as support of electronic circuits are highly desired [8–11]. Poly(vinylidene fluoride) (PVDF) is widely used as a polymer matrix due to its high ϵ' of about 10 compared to other polymers [1, 11–14].

Usually, the simple and effectively method to obtain enhanced ϵ' value of flexible polymer-based composites is the incorporation of high-permittivity ceramic particles into polymer matrix. The common ceramic fillers used are BaTiO_3 [5, 13, 15–17], $(\text{Ba}_{0.6}\text{Sr}_{0.4})\text{TiO}_3$ [18–20], $\text{CaCu}_3\text{Ti}_4\text{O}_{12}$ (CCTO) [21–23], $\text{Na}_{0.5}\text{Bi}_{0.5}\text{Cu}_3\text{Ti}_4\text{O}_{12}$ [24], and $\text{Ba}(\text{Fe}_{0.5}\text{Nb}_{0.5})\text{O}_3$ [25]. Although significant efforts have been made for increasing ϵ' of these ceramic/polymer composite systems, ϵ' values these composites are difficult to significantly enhance by more than 100, in which 50 vol% ceramic particles was filled in. Furthermore, the ferroelectric ceramics usually exhibit piezoelectric effect, which results in a mechanical resonance in the device during charging and discharging. This can cause the reliability limit of the fabricated device. In addition, some ferroelectric ceramics consists of Pb, which might contaminate the environment.

Considering nanosized ceramic fillers, large interfacial areas and very short interparticle distance in the composites containing nanosized fillers promote the exchange coupling

✉ Prasit Thongbai
pthongbai@kku.ac.th

¹ Materials Science and Nanotechnology Program, Faculty of Science, Khon Kaen University, Khon Kaen 40002, Thailand

² Integrated Nanotechnology Research Center (INRC), Department of Physics, Faculty of Science, Khon Kaen University, Khon Kaen 40002, Thailand

³ School of Physics, Institute of Science, Suranaree University of Technology, Nakhon Ratchasima 30000, Thailand

⁴ Sustainable Infrastructure Research and Development Center, Department of Civil Engineering, Faculty of Engineering, Khon Kaen University, Khon Kaen 40002, Thailand

effect through a dipolar interface layer. This results in a significantly enhanced polarization intensity and thus ϵ' [26], which offers greater possibilities to tailor and optimizes the properties of polymer based composites compared to those of microsized ceramic fillers. Nanosized fillers can decrease the possibility of porosity in polymer matrix composite, leading to a better microstructure. For practical applications, moreover, nanoparticles would reduce the dimensions of composites and increase the packing density [25].

Most recently, we found that $\text{Na}_{1/3}\text{Ca}_{1/3}\text{Bi}_{1/3}\text{Cu}_3\text{Ti}_4\text{O}_{12}$ (NCB), a new giant dielectric perovskite ceramic in $\text{ACu}_3\text{Ti}_4\text{O}_{12}$ compounds, has better dielectric properties compared to that of $\text{CaCu}_3\text{Ti}_4\text{O}_{12}$. High $\epsilon' \approx 2.5 \times 10^4$ and low $\tan\delta \approx 0.038$ at 1 kHz with good temperature stability were notably achieved in the NCB ceramic. Therefore, in this work, nanosized-NCB/PVDF nanocomposites were prepared. The effects of nanosized filler on the microstructure and dielectric properties were investigated. It was found that the largely enhanced ϵ' of about 528 (210) at 100 Hz (1 kHz) with retaining low $\tan\delta$ in PVDF polymer matrix nanocomposite was successfully obtained by filling with 50 vol% nanosized-NCB.

2 Experimental details

2.1 Preparation of $\text{Na}_{1/3}\text{Ca}_{1/3}\text{Bi}_{1/3}\text{Cu}_3\text{Ti}_4\text{O}_{12}$

Nanosized- $\text{Na}_{1/3}\text{Ca}_{1/3}\text{Bi}_{1/3}\text{Cu}_3\text{Ti}_4\text{O}_{12}$ powder (NCB-NP) was prepared by a chemical combustion (CC) method using urea as fuel. $\text{Ca}(\text{NO}_3)_2 \cdot 4\text{H}_2\text{O}$ (99 %, Sigma–Aldrich), NaNO_3 (99.99 %, Kanto Chemical), $(\text{CH}_3\text{CO}_2)_3\text{Bi}$ (99.99 %, Sigma–Aldrich), $\text{Cu}(\text{NO}_3)_2 \cdot 4\text{H}_2\text{O}$ (99.5 %, Carlo Erba), $\text{C}_{16}\text{H}_{28}\text{O}_6\text{Ti}$ (75 wt% in isopropanol, Sigma–Aldrich), acetic acid, deionized water, and urea were used as starting raw materials. Details of the preparation method are given elsewhere [27]. First, stoichiometric amounts of $\text{Ca}(\text{NO}_3)_2 \cdot 4\text{H}_2\text{O}$, NaNO_3 , $(\text{CH}_3\text{CO}_2)_3\text{Bi}$, and $\text{Cu}(\text{NO}_3)_2 \cdot 4\text{H}_2\text{O}$ were dissolved in an aqueous solution of acetic acid. Second, a $\text{C}_{16}\text{H}_{28}\text{O}_6\text{Ti}$ solution was slowly dropped into the metal ion solution under constant stirring until the formation of a clear and transparent solution was obtained. Then, urea powder was added into the mixed solution with stirring at 150 °C until a viscous gel formed. The gel was dried in air at 350 °C for 30 min. The resulting dried porous precursor was ground and calcined at 750 °C for 4 h. The obtaining NCB-NPs were achieved. Micro- $\text{Na}_{1/3}\text{Ca}_{1/3}\text{Bi}_{1/3}\text{Cu}_3\text{Ti}_4\text{O}_{12}$ powder (NCB-MP) was prepared by a solid state reaction (SSR) method. The mixture of starting powders was mixed by ball milling in ethanol and calcined at 950 °C for 5 h.

2.2 Preparation of NCB/PVDF composites

The NCB-NPs and NCB-MPs were used as filler in PVDF (Sigma–Aldrich Co., France) matrix. The NCB/PVDF composites with different volume fractions of NCB ($f_{\text{NCB}} = 0, 0.1, 0.2, 0.3, 0.4,$ and 0.5) were prepared by a liquid-phase assisted dispersion method. First, NCB and PVDF particles were mixed by ball-milling in absolute ethanol for 30 min using ZrO_2 balls. Second, the mixture of NCB and PVDF particles was further dried to evaporate absolute ethanol. Finally, the dry mixture powders were molded by hot-pressing at about 200 °C for 30 min under 10 MPa. The final composite samples with a disc-shape are 12 mm in diameter and 1 mm in thickness.

2.3 Characterization techniques

X-ray diffraction (XRD; Bruker, D2 phaser) was used to characterize the phase compositions and crystal structures of the NCB-NPs and NCB-MPs and NCB/PVDF composites. Scanning electron microscopy (SEM) (SEM; LEO 1450VP; Cambridge, UK) and field-emission scanning electron microscopy (FE-SEM) were used to characterize nanosized NCB powders and NCB/PVDF nanocomposites. For the dielectric measurement, surfaces of the nanocomposite samples were painted by silver past. The capacitance (C_p) and dissipation factor ($\tan\delta$) of the polymeric composite samples were measured using an Agilent 4294A Precision Impedance Analyzer over the frequency range of 10^2 – 10^7 Hz at room temperature with an oscillation voltage of 500 mV.

3 Results and discussion

Figure 1 shows the SEM images of the NCB-NPs and NCB-MPs powders prepared by CC and SSR methods, respectively. Obviously, the particle sizes of the NCB-NPs and NCB-MPs powders are of about 100–200 nm and 1–2 μm , respectively. An agglomeration of both powders is observed. The XRD patterns of the NCB-NPs and NCB-MPs powders are illustrated in Fig. 2. The main phase of NCB is detected in both powders. These XRD patterns are similar to that of CCTO structure (JCPDS 75-2188) with *bcc* structure. However, a small amount of CuO secondary phase is still observed in the XRD pattern of the NCB-NPs powder.

As depicted in the inset of Fig. 3, it is found that the co-existence of α - and γ -phase of PVDF was confirmed [8]. This result is similar to that observed in the $\text{Na}_{1/2}\text{Bi}_{1/2}\text{Cu}_3\text{Ti}_4\text{O}_{12}$ /PVDF composites [24]. Figure 3 demonstrates the XRD patterns of NCB-NPs/PVDF nanocomposites with different loading contents of nanofiller. All XRD peaks of

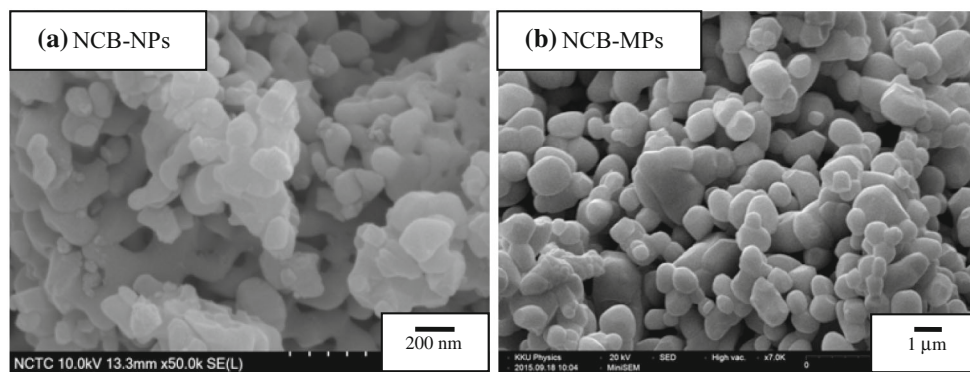


Fig. 1 SEM images of **a** NCB-NPs and **b** NCB-MPs

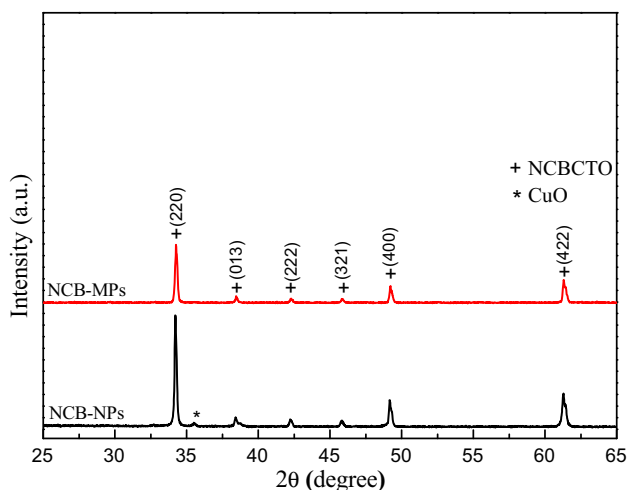


Fig. 2 XRD patterns of NCB-NPs and NCB-MPs

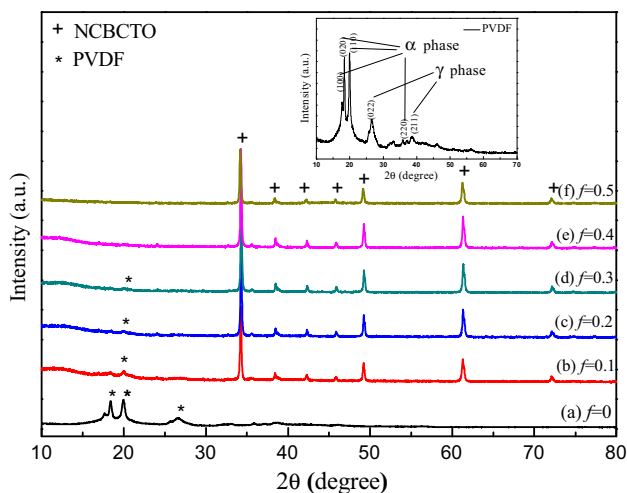


Fig. 3 XRD patterns of NCB-NPs/PVDF nanocomposites with different volume fractions of NCB-NPs ($f = 0$ – 0.5); inset illustrates the XRD pattern of PVDF

the NCB-NPs/PVDF nanocomposites are perfectly indexed as *bcc* structure. XRD peak of PVDF is observed in the composites with low loading content of filler. The XRD patterns of NCB-NPs are unchanged for all compositions. The intensities of PVDF-phase diffraction peaks decrease with increasing NCB-NPs content in the nanocomposites.

The effect of particle sizes of filler on the microstructure of NCB/PVDF polymer composites is shown in Fig. 4. Figures 4a–b reveal the fractured cross section of the NCB-NPs/PVDF nanocomposites. The dispersion of NCB-NPs in the PVDF matrix is quite good. Figures 4c–d show the cross section of the NCB-MPs/PVDF composites. Pores are observed in the NCB-MPs/PVDF composites. It is observed that NCB-NPs and NCB-MPs are randomly surrounded by the polymer matrix, indicating that 0–3 connectivity pattern is formed [1, 25]. For the nanocomposite with 50 vol% (Fig. 4b), NCB-NPs are dispersed homogeneously in the PVDF matrix with small trails of aggregation. In contrast, as the NCB-MPs filler content increases, a large amount of pores can be observed in the NCB-MPs/PVDF composite with 50 vol% NCB-MPs. The porosity resulted from high loading would have a great impact on the dielectric properties of the polymer composites. Usually, the dispersion of fillers would play a significant role on dielectric properties of composites and good dispersion is likely to contribute to excellent dielectric properties [1, 13]. Accordingly, these results indicate the better performance the NCB-NPs on the microstructure of the polymer composites.

The dielectric properties of the NCB-NPs/PVDF nanocomposites are shown in Figs. 5 and 6. ϵ' of NCB-NPs/PVDF nanocomposites increases with increasing $f_{\text{NCB-NPs}}$. Note that ϵ' of NCB-MPs/PVDF composites also increased as $f_{\text{NCB-MPs}}$ was increased. As demonstrated in Fig. 5, ϵ' of the NCB-NPs/PVDF nanocomposites with $f_{\text{NCB-NPs}} \leq 0.2$ is slightly dependent on frequency in the

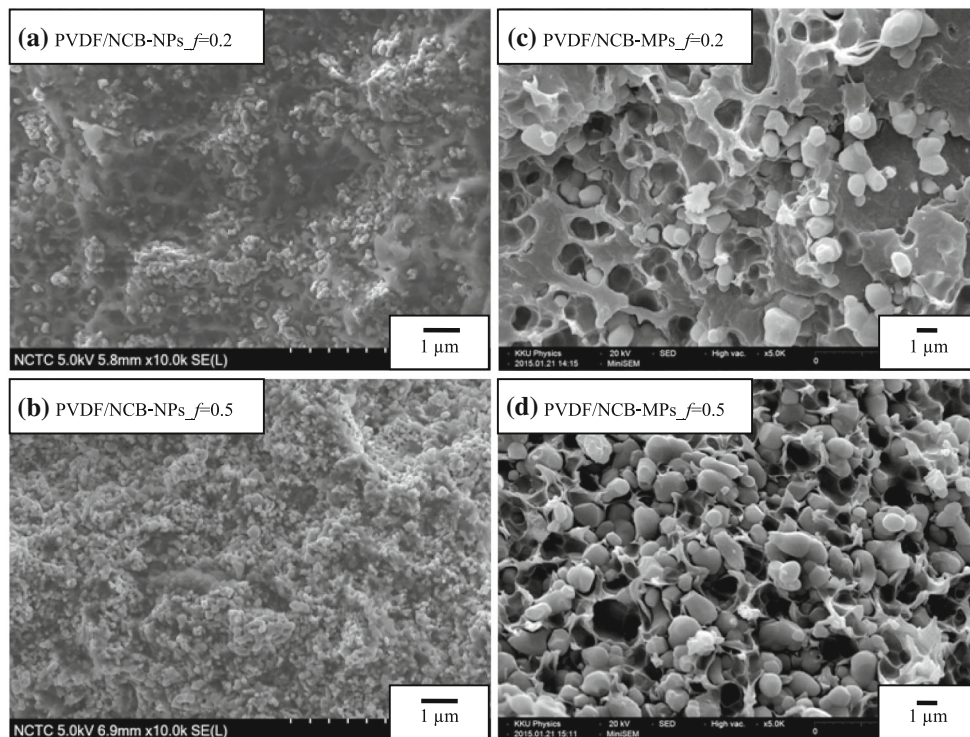


Fig. 4 SEM images of **a–b** NCB-NPs/PVDF and **c–d** NCB-MPs with $f = 0.2$ and 0.5

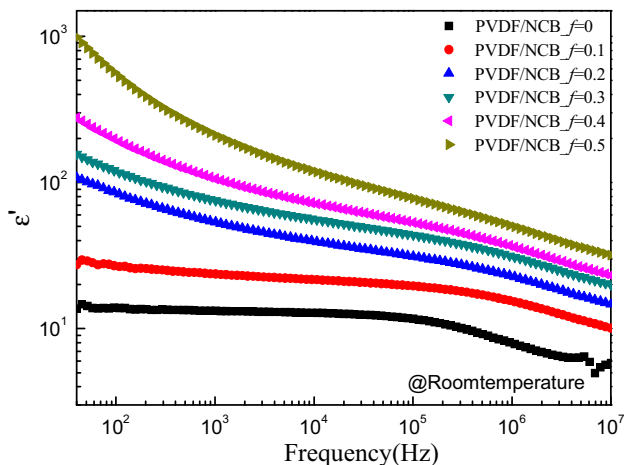


Fig. 5 ϵ' as a function of frequency at room temperature of NCB-NPs/PVDF nanocomposites

range of 40– 10^7 Hz. In the low-frequency range, ϵ' of NCB-NPs/PVDF nanocomposites with $f_{\text{NCB-NPs}} \geq 0.2$ is strongly dependent on frequency. This evidently indicates that the dielectric response is primarily caused by the interfacial polarization effect. As the concentration of NCB-NPs fillers was increased to $f_{\text{NCB-NPs}} = 0.1, 0.2, 0.3, 0.4,$ and 0.5 , the values of ϵ' at 10^3 Hz increased to 23.7, 53.4, 75.3, 105.9, and 210.8, respectively. It is worth noting that for the nanocomposite with $f_{\text{NCB-NPs}} = 0.5$, the ϵ' at 10^2 and

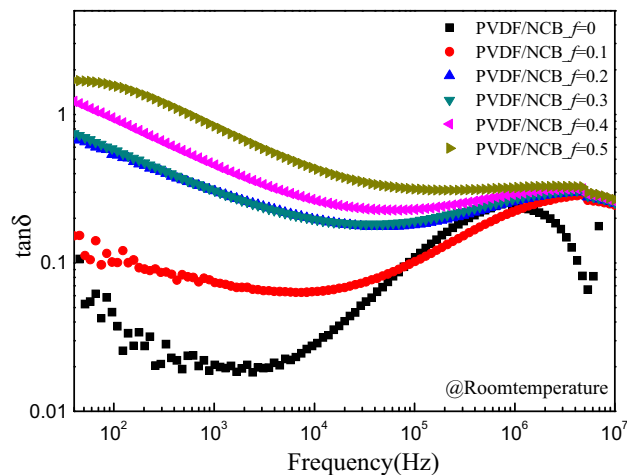


Fig. 6 $\tan\delta$ as a function of frequency at room temperature of NCB-NPs/PVDF nanocomposites

10^3 Hz is, respectively, 50 and 20 times higher than that of pure PVDF polymer.

The frequency dependence of $\tan\delta$ at room temperature of the NCB-NPs/PVDF nanocomposites is illustrated in Fig. 6. In the frequency range of 40– 10^5 Hz, $\tan\delta$ of the NCB-NPs/PVDF nanocomposites increases with increasing NCB-NPs loading content. It is observed that $\tan\delta$ of all nanocomposite samples decreases in the frequency range of 40– 10^4 Hz, and then tends to increase over 10^4 Hz. The

dielectric response in a low-frequency range is a typical interface polarization behavior. This was resulted from macroscopical heterogeneous interface of the different diphase structures [1]. On the other hand, the high-frequency dielectric response is a Debye relaxation behavior derived from the C-F dipole orientation polarization of PVDF matrix [25]. Interestingly, at 1 kHz, the nanocomposite with $f_{\text{NCB-NPs}} = 0.5$ can exhibit good dielectric properties with high ϵ' of about 210.8 and low $\tan\delta \approx 0.83$. This high ϵ' value is much larger than those of observed in the CCTO/PVDF [21] and $\text{Na}_{1/2}\text{Bi}_{1/2}\text{Cu}_3\text{Ti}_4\text{O}_{12}$ /PVDF composites [27].

Generally, the dispersion of fillers would play a significant role on dielectric properties of composites and good dispersion is likely to contribute to excellent dielectric properties [1]. As revealed in Fig. 4, the NCB-NPs are good dispersed in the PVDF polymer matrix. Furthermore, porosity in the NCB-NPs/PVDF nanocomposites is very low compared to that of the NCB-MPs/PVDF composites. According to the microstructure analysis, ϵ' of the NCB-NPs/PVDF nanocomposites should therefore be better than that of the NCB-MPs/PVDF composites. As clearly seen in Fig. 7, the ϵ' value of each NCB-NPs/PVDF composition is larger than that of the NCB-MPs/PVDF composite. Another important reason is that the high ϵ' of NCB-NPs/PVDF nanocomposites is dominantly caused by enhanced interfacial polarization. This primarily originates in the significant blocking of charge carriers at internal interfaces (i.e., the Maxwell–Wagner–Sillars effect) under an electric field due to the formation of a large number of interfaces between NCB-NPs and PVDF polymer matrix. By comparing the NCB-NPs and NCB-MPs ceramic fillers, larger interfacial areas and hence very shorter interparticle distance in the nanocomposites can cause the great exchange coupling effect through a dipolar interface layer. This

results in a significantly enhanced ϵ' as a result of an increased polarization intensity [26].

4 Conclusions

In conclusion, ϵ' of PVDF polymer was greatly enhanced by incorporating with NCB-NPs. It was found that the dispersion of NCB-NPs in PVDF matrix was quite good. The NCB-NPs/PVDF nanocomposite with $f_{\text{NCB-NPs}} = 0.5$ exhibited high ϵ' of about 210.8 with low $\tan\delta \approx 0.83$. This increased ϵ' value was much larger than that of PVDF polymer by a factor of ≈ 20 . It was also found that the ϵ' value of the NCB-NPs/PVDF was much larger than that of the NCB-MPs/PVDF microcomposites. Very high ϵ' of the NCB-NPs/PVDF nanocomposites was originated from the large interfacial areas coupled with very short interparticle distance.

Acknowledgments This work was financially supported by the Thailand Research Fund (TRF) and Khon Kaen University under the TRF Senior Research Scholar Contract No. RTA5780004. P. Kumonsa would like to thank the Science Achievement Scholarship of Thailand (SAST) for her Master of Science Degree scholarship.

References

1. Z.-M. Dang, J.-K. Yuan, J.-W. Zha, T. Zhou, S.-T. Li, G.-H. Hu, *Prog. Mater. Sci.* **57**, 660 (2012)
2. P. Martins, A.C. Lopes, S. Lanceros-Mendez, *Prog. Polym. Sci.* **39**, 683 (2014)
3. D. Wang, Y. Bao, J.-W. Zha, J. Zhao, Z.-M. Dang, G.-H. Hu, *ACS Appl. Mater. Interfaces* **4**, 6273 (2012)
4. T. Li, J. Chen, H. Dai, D. Liu, H. Xiang, Z. Chen, *J. Mater. Sci. Mater. Electron.* **26**, 312 (2014)
5. M.-F. Lin, V.K. Thakur, E.J. Tan, P.S. Lee, *RSC Adv.* **1**, 576 (2011)
6. P. Thakur, A. Kool, N.A. Hoque, B. Bagchi, S. Roy, N. Sepay, S. Das, P. Nandy, *RSC Adv.* **6**, 26288 (2016)
7. X. Lin, P. Hu, Z. Jia, S. Gao, *J. Mater. Chem. A* **4**, 2314 (2016)
8. A. Paleo, C. Martínez-Boubeta, L. Balcells, C. Costa, V. Sencadas, S. Lanceros-Mendez, *Nanoscale Res. Lett.* **6**, 257 (2011)
9. Q. Xiao, L. Li, B.Q. Zhang, X.M. Chen, *Ceram. Int.* **39**, S3 (2013)
10. Y. Song, Y. Shen, H. Liu, Y. Lin, M. Li, C.-W. Nan, *J. Mater. Chem.* **22**, 16491 (2012)
11. N. Levi, R. Czerw, S. Xing, P. Iyer, D.L. Carroll, *Nano Lett.* **4**, 1267 (2004)
12. J. Bi, Y. Gu, Z. Zhang, S. Wang, M. Li, Z. Zhang, *Mater. Des.* **89**, 933 (2016)
13. K. Silakaew, W. Saijingwong, K. Meeporn, S. Maensiri, P. Thongbai, *Microelectron. Eng.* **146**, 1 (2015)
14. K. Yu, H. Wang, Y. Zhou, Y. Bai, Y. Niu, *J. Appl. Phys.* **113**, 034105 (2013)
15. T. Zhou, J.-W. Zha, R.-Y. Cui, B.-H. Fan, J.-K. Yuan, Z.-M. Dang, *ACS Appl. Mater. Interfaces* **3**, 2184 (2011)
16. L. Xie, X. Huang, Y. Huang, K. Yang, P. Jiang, *ACS Appl. Mater. Interfaces* **5**, 1747 (2013)
17. Y.K. Jang, J.C. Won, H.G. Yoon, *Appl. Phys. Lett.* **95**, 052907 (2009)

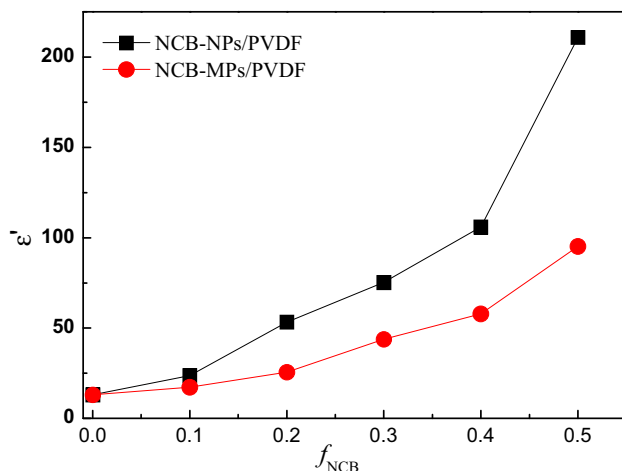


Fig. 7 ϵ' as a function of volume fraction at room temperature and 1 kHz of NCB-NPs and NCB-MPs

18. K. Li, H. Wang, F. Xiang, W. Liu, H. Yang, *Appl. Phys. Lett.* **95**, 202904 (2009)
19. W. Xia, Z. Xu, F. Wen, Z. Zhang, *Ceram. Int.* **38**, 1071 (2012)
20. Y. Song, Y. Shen, P. Hu, Y. Lin, M. Li, C.W. Nan, *Appl. Phys. Lett.* **101**, 152904 (2012)
21. P. Thomas, K.T. Varughese, K. Dwarakanath, K.B.R. Varma, *Compos. Sci. Technol.* **70**, 539 (2010)
22. Y. Shen, A. Gu, G. Liang, L. Yuan, *Compos. A Appl. Sci. Manuf.* **41**, 1668 (2010)
23. B.S. Prakash, K.B.R. Varma, *Compos. Sci. Technol.* **67**, 2363 (2007)
24. Y.-L. Su, C. Sun, W.-Q. Zhang, H. Huang, *J. Mater. Sci.* **48**, 8147 (2013)
25. Z. Wang, M. Fang, H. Li, Y. Wen, C. Wang, Y. Pu, *Compos. Sci. Technol.* **117**, 410 (2015)
26. K.S. Deepa, M.T. Sebastian, J. James, *Appl. Phys. Lett.* **91**, 202904 (2007)
27. W. Tuichai, P. Thongbai, V. Amornkitbamrung, T. Yamwong, S. Maensiri, *Microelectron. Eng.* **126**, 118 (2014)